An efficacious and safe rescue of GM3 synthase deficiency by spatially regulated rAAV-mediated *ST3GAL5* delivery

Huiya Yang
University of Massachusetts Chan Medical School
Robert Brown
University of Massachusetts Medical School https://orcid.org/0000-0001-6062-1528
Dan Wang
University of Massachusetts Chan Medical School https://orcid.org/0000-0001-9079-2360
Kevin Strauss
Guangping Gao (Guangping.Gao@umassmed.edu)
University of Massachusetts Chan Medical School https://orcid.org/0000-0003-0097-9012

Article

Keywords:

Posted Date: June 17th, 2022

DOI: https://doi.org/10.21203/rs.3.rs-1731386/v1

Abstract

GM3 synthase deficiency (GM3SD) is an infantile-onset epileptic encephalopathy syndrome caused by biallelic loss-of-function mutations in *ST3GAL5.* Loss of ST3GAL5 activity in humans results in systemic ganglioside deficiency and severe neurological impairment. No disease-modifying treatment is currently available. Certain recombinant adeno-associated viruses (rAAVs) are capable of crossing the blood-brain barrier to induce widespread, long-term gene expression in the central nervous system (CNS), and represent a promising therapeutic strategy. Here, we show that a first-generation rAAV-*ST3GAL5* replacement vector employing a ubiquitous promoter restored tissue ST3GAL5 expression and normalized cerebral gangliosides in patient-derived iPSC neurons and brain tissue from *St3gal5* knock-out mice, but caused fatal hepatotoxicity when administered systemically. In contrast, a second-generation vector optimized for CNS-restricted ST3GAL5 expression, administered by either intracerebroventricular or intravenous route, allowed for safe and effective rescue of lethality and neurological impairment in murine models of GM3SD. These results support further clinical development of *ST3GAL5* gene therapy.

One Sentence Summary

A spatially controlled rAAV-mediated *ST3GAL5* gene delivery to CNS evades off-target hepatotoxicity and achieves a marked amelioration of abnormalities in GM3 synthase deficiency mouse models.

Introduction

ST3GAL5 encodes GM3 synthase (ST3GAL5; a.k.a. GM3S and SIAT9), the rate-limiting enzyme for production of all a- and b-series gangliosides normally enriched in mammalian brain (Fig. 1A) (*1–6*). Biallelic *ST3GAL5* loss-of function variants result in systemic ganglioside deficiency, an infantile-onset neurodevelopmental syndrome characterized by intractable epileptic encephalopathy, auditory and visual impairment, global psychomotor delay, extrapyramidal movements, and untimely death. A number of pathogenic variants have been linked to the GM3 synthase deficiency syndrome (GM3SD) in populations worldwide (*2, 7*). Within Old Order Amish communities of North America, the incidence of GM3SD is enriched to approximately 1 per 1,200 births due to a severe *ST3GAL5* c.862C > T (p.Arg288Ter) founder variant that abrogates ST3GAL5 activity and results in absence of GM3 and its most important downstream products, GM1, GD1a, GD1b, and GT1b (*3*).

GM3 and derivative a- and b-series gangliosides are expressed in cytosolic membranes of all mammalian cells, where they contribute to microdomain architecture and activity of intramembrane proteins (*cis* interactions), as well as ligand binding and intercellular contacts (*trans* interactions) (*8*). Disrupted ganglioside synthesis results in neurotoxicity from multiple overlapping mechanisms, including altered receptor interactions, abnormal cellular membrane dynamics, and reduced mitochondrial membrane potential and oxygen consumption (*4, 9*). Oral ganglioside replacement therapy via a powdered buttermilk supplement (G500; Aukland, New Zealand) may transiently improve growth and development during

infancy, but low enteral absorption of gangliosides and their restricted transit across the blood-brain barrier (BBB) may ultimately limit the utility of dietary therapy, leading to treatment failures and loss of long-term efficacy (*10*). At present, no other effective treatment is available for GM3SD.

The development of novel and robust therapeutic modalities requires testing in proper animal models that genetically and phenotypically recapitulate human GM3SD. Homozygous *St3gal5*$^{-/-}$ mice exhibit a- and b-series ganglioside deficiency, insulin hypersensitivity, and hearing loss, but in contrast to human patients, do not suffer from early mortality or clinically relevant neurological disease (*11, 12*). In mice, biochemical defects caused by ST3GAL5 deficiency seem to be compensated by remaining minor gangliosides species, resulting in minimal physiological alternations (Fig. 1A). However, mice with knockout of both *St3gal5* and *B4galnt1* are unable to synthesize any gangliosides and more closely mirror clinical hallmarks such as CNS pathology, developmental delay, motor impairment, and early death (**Fig. S1**) (*13*). Thus, *St3gal5* single knockout and *St3gal5/B4galnt1* double knockout mice serve as complementary models for evaluating the actions of novel therapies.

Because GM3SD is a monogenic loss-of-function disease, gene replacement therapy may be a promising approach. Recombinant adeno-associated viruses (rAAVs) have emerged as powerful gene delivery tools for the treatment of monogenic diseases, and to date have been tested in 17 clinical trials targeting CNS disorders (*14, 15*). An ideal rAAV vector should deliver its therapeutic cargo into specific target cells to restore an appropriate spatial, quantitative, and temporal pattern of protein expression. However, a limiting factor for successful and safe rAAV-mediated gene therapy is the broad tropism of common AAV serotypes. The naturally isolated AAV serotype 9 (AAV9) is able to cross the BBB and transduce neural tissues, but also efficiently transduces multiple peripheral tissues such as liver, skeletal muscle, and heart (*16, 17*). Hepatoxicity after high dose systemic AAV9 delivery (*18, 19*), including several patient deaths due to acute liver failure (*20, 21*), has raised legitimate concerns about the overall safety of gene therapy. Therefore, regulating the tissue specificity of transgene delivery and expression may preserve the therapeutic benefits of rAAV while minimizing associated risks. Currently, this can be approached through a combination of variables, including route of administration (e.g., regional tissue injection), use of CNS-favorable viral capsids, and inclusion of cell type-specific promoters and tissue de-targeting microRNA binding sites within the therapeutic genome sequence.

In this study, we first examined *ST3GAL5* replacement cassettes for their ability to reconstitute gangliosides in cortical neurons produced from GM3SD patient-derived induced pluripotent stem cells (iPSCs). We then administered the AAV9 vectors by intracerebroventricular (ICV) injection to *St3gal5*$^{-/-}$ and *St3gal5*$^{-/-}$*/B4galnt1*$^{-/-}$ mice. Treatment with rAAV9-*ST3GAL5* extended survival, restored CNS ganglioside production, improved growth, and partially rescued motor function of experimental animals. When delivered systemically, however, this therapy led to hepatic injury and death caused by high off-target ST3GAL5 expression in the liver. We therefore designed a second-generation rAAV9 vector using a CNS-specific promoter (human Synapsin1) in combination with liver-specific microRNA targeting sequences (miR-122) to optimize both transcriptional and post-transcriptional regulation (*22, 23*). In GM3SD mouse models, this strategy eliminated liver toxicity while preserving neurotherapeutic effects.

Finally, we examined if data from the *St3gal5*$^{-/-}$/*B4galnt1*$^{-/-}$ double knockout mouse underrepresented the therapeutic potential of GM3SD gene therapy as it might apply to humans, and therefore co-injected *St3gal5*$^{-/-}$/*B4galnt1*$^{-/-}$ mice with both *ST3GAL5* and *B4GALNT1* rAAV vectors. Vector co-injection completely eliminated neurological signs of disease in *St3gal5*$^{-/-}$/*B4galnt1*$^{-/-}$ mice and this was achieved by either ICV delivering of AAV9 vectors or systemically delivering of PHP.eB vectors, which exhibit unusually efficient transit across the murine BBB. Overall, our study illuminates a path for translating safe and effective *ST3GAL5* gene therapy to clinical trials.

Results

ST3GAL5 **transgene design and** in vitro **expression**

ST3GAL5-1a-2 (NM_003896) is the most abundant messenger RNA (mRNA) among four *ST3GAL5* mRNA variants in the human brain (Fig. 1B) (*24–26*); we thus focused on this variant for further vector development. The first AUG start codon in *ST3GAL5-1a-*2 is in a weak translation initiation context (AUUAGUAUGC). Most ribosomes therefore skip the first AUG and recognize either of two downstream AUG as the start codon (*27, 28*). As a result, three ST3GAL5 protein isoforms differing in their N-termini are produced (Fig. 1B). Due to the lack of knowledge about their physiological roles, we designed and tested different human *ST3GAL5* replacement constructs carrying each open reading frame (Fig. 1B). The codon-optimized transgenes were cloned into a ubiquitous expression cassette driven by chicken beta-actin (CB) promoter with an intron (Fig. 1C), and transfected into HeLa cells to confirm protein expression. We found that expression of the shortest construct (ORF3) was weak, and adding Kozak sequence GCCACC (construct KORF3) greatly enhanced expression (Fig. 1D).

We next evaluated whether these *ST3GAL5* constructs could function in ganglioside synthesis in cultured neurons. To this end, we differentiated normal (*ST3GAL5*$^{+/+}$) and patient (*ST3GAL5*$^{E332K/E332K}$) iPSCs into cortical neurons (Fig. 2A-2B), infected them with lentiviral vectors expressing different *ST3GAL5* isoforms. While major brain gangliosides (GD1a, GD1b, and GT1b) were absent in untreated patient neurons, they were restored following transduction of any *ST3GAL5* isoform (Fig. 2C) (*29*). We focused on the KORF3 transgene design in future development, because its small gene size (1,095 base pairs) is amenable to the self-complementary AAV vector design that can further enhance vector potency when packaging capacity is limited (< 2.5 kb).

Intracerebroventricular injection of rAAV9-ST3GAL5.v1 improved biochemical and phenotypic abnormalities in GM3SD mouse models

Encouraged by *in vitro* results, we generated AAV9 vector carrying a CB promoter-driven *ST3GAL5* construct (rAAV9-ST3GAL5.v1) to assess therapeutic efficacy in mice following *in vivo* delivery. We first treated *St3gal5*$^{-/-}$ mice by unilateral intracerebroventricular (ICV) injection of $3x10^{10}$ genome copies

(gc)/pup at postnatal day 1 (P1), and euthanized animals 4 weeks post-injection (Fig. 3A). The *ST3GAL5* transgene was detected in brain, liver, and heart, where it induced tissue mRNA expression in excess of endogenous levels (Fig. 3B). GM3 and its derivatives (GM2, GD1a, and GD1b) were undetectable in the *St3gal5*$^{-/-}$ brain. ICV injection of rAAV9-ST3GAL5.v1 restored these a- and b-series gangliosides to WT levels, concomitant with substantial clearance of lactosylceramide (LacCer), the proximate substrate for GM3 synthase (Fig. 3C-3D, S2). However, ganglioside deficiency persisted in serum, likely because vector genomes delivered by ICV injection did not sufficiently penetrate peripheral tissues (**Fig. S3**). Because gangliosides are 10- to 30-fold more abundant in human brain as compared to any other tissue (*30*), we postulated that ganglioside restoration in CNS was the key to preventing neurological morbidity in GM3SD animals.

St3gal5 $^{-/-}$ mice have hearing loss but do not exhibit many of the other neurological deficits characteristic of GM3SD in humans. For testing vector effectiveness, we therefore used the *St3gal5*$^{-/-}$*/B4galnt1*$^{-/-}$ mouse model, which models key aspects of the human GM3SD phenotype, including reduced survival, growth failure, motor impairments, and neuropathology. These animals were benchmarked to *St3gal*$^{+/-}$*/B4galnt1*$^{-/-}$ mice, which did not exhibit significant neurological morbidity during the period of experimental observation (**Fig. S4A**). ICV administration of rAAV9-ST3GAL5.v1 to newborn *St3gal5*$^{-/-}$*/B4galnt1*$^{-/-}$ pups (3x10^{10} gc, P1) extended their survival up to 300 days (median survival: untreated, 18 days; treated, 56 days) (**Fig. S4B**), improved growth, and partially restored motor function as assessed by the negative geotaxis test (**Fig. S4C-F**). Taken together, these results demonstrated that neonatal ICV injection of rAAV9-ST3GAL5.v1 was well tolerated and could restore endogenous cerebral ganglioside production, but did not fully alleviate GM3SD disease in *St3gal5*$^{-/-}$*/B4galnt1*$^{-/-}$ mice.

Systemic delivery of rAAV9-ST3GAL5.v1 caused liver toxicity

While ICV injection considerably reduced disease burden in murine models, we wondered if systemic delivery could have further advantages. Specifically, systemic vector delivery has the potential to more broadly and evenly distribute AAV9 vector throughout the neuraxis, taking advantage of a naturally dense capillary network that perfuses the mammalian CNS (*31*), and could deliver therapeutic genomes to peripheral neural tissues (e.g., peripheral nerve axons and Schwann cells) that express, and may be functionally dependent upon, complex gangliosides (*32–34*). Accordingly, we administered rAAV9-ST3GAL5.v1 to P1 *St3gal5*$^{-/-}$ pups by facial vein injection using 3x10^{11} gc/pup, and treated *St3gal5*$^{+/+}$ littermates in parallel as controls. All treated mice unexpectedly died within 3 days post-injection, regardless of genotype (Fig. 4A). In order to understand fatality, we injected wildtype pups with therapeutic vector, capsids containing cDNA for enhanced green fluorescent protein (EGFP), empty capsids (AAV9.empty), or phosphate-buffered saline (PBS) (Fig. 4B). We found that in WT mice systemically treated with rAAV9-ST3GAL5.v1, expression of *ST3GAL5* in liver was elevated more than 100-fold relative to mouse endogenous *St3gal5* level (Fig. 4C), accompanied by activation of cellular

death and defense response (Fig. 4D-4E). We confirmed RNAseq results with qPCR and ELISA, which revealed consistent activation of pro-inflammatory cytokines (TNFα, IL1α, CCL2, and CCL3) (**Fig. S5A-S5B**). These molecular changes were accompanied by cellular liver pathology, including hepatocyte swelling (Fig. 4F) and cell death (Fig. 4G). We thus speculated that overexpression of *hST3GAL5* transgene in liver and its attendant cytopathic effects played a direct role in lethal toxicity of systemically administered rAAV9-ST3GAL5.v1.

Optimized ST3GAL5 vector construct with spatial regulation eliminated liver toxicity associated with systemic administration

We reasoned that CNS-restricted and liver-detargeted expression of an *ST3GAL5* transgene might preserve therapeutic efficacy while eliminating hepatotoxicity. We therefore designed a spatially regulated expression cassette that included human Synapsin 1 (Syn1) promoter (*35, 36*) to drive neuronal expression at the transcriptional level, combined with miR-122 binding sites in the 3' untranslated region (UTR), which silence transgene expression in hepatocytes at the post-transcriptional level (Fig. 4C) (*22, 23*). We named this refined construct ST3GAL5.v2 and packaged it into AAV9. Following the same P1 facial vein injection paradigm in WT pups, transgene expression from rAAV9-ST3GAL5.v2 was greatly reduced in liver tissue and all animals survived with no evidence of liver inflammation, cytopathology, or transcriptomic derangements (Fig. 4, **Fig. S5**).

Interestingly, we noticed that packaging the first-generation construct (rAAV9-ST3GAL5.v1) consistently resulted in low titers (1 to $4x10^{12}$ gc/mL), likely due to transgene toxicity in HEK293 cells during the manufacturing process. In contrast, rAAV9-ST3GAL5.v2 was routinely produced at higher titers of 0.8 to $1.5x10^{13}$ gc/mL (**Fig. S6**). We therefore concluded that by tuning tissue specificity, the optimized second-generation construct design eliminated both hepatotoxicity and the manufacturing bottleneck, serving as a clinically translatable candidate for studies that followed.

ICV injection of rAAV9-ST3GAL5.v2 improved biochemical and phenotypic abnormalities in GM3SD mouse models

We cloned the ST3GAL5.v2 construct in self-complementary (sc) configuration to facilitate faster and stronger expression as compared to the single-stranded (ss) transgene (Fig. 5A) (*37, 38*). Following P1 ICV injection in *St3gal5*$^{-/-}$ mice, scAAV9- and ssAAV9-ST3GAL5.v2 led to comparable levels of transgene expression in hippocampus four weeks post-injection, whereas scAAV9 slightly outperformed ssAAV9 in the cerebral cortex (Fig. 5B). Both vectors normalized the brain ganglioside profile in *St3gal5*$^{-/-}$ mice up to 12 weeks post-injection (Fig. 5C-5D), although neither corrected circulating gangliosides, consistent with the neuron-specific expression design (**Fig. S7**).

Using the same P1 ICV injection paradigm, we next treated *St3gal5*$^{-/-}$/*B4galnt1*$^{-/-}$ pups with either scAAV9- or ssAAV9-ST3GAL5.v2 (Fig. 6A). Both vectors significantly extended animal survival (median survival: untreated, 19 days; ssAAV9, 51 days; scAAV9: 101 days) (Fig. 6B), partially restored body growth (Fig. 6C-6D), and largely normalized motor function as revealed by negative geotaxis and rotarod tests

(Fig. 6E-6F**)**. Importantly, both treatments improved brain growth (Fig. 6G) while reducing or eliminating neuropathological changes such as cerebellar vacuolization (Fig. 7A), neuronal cell death (Fig. 7B), and astrogliosis (Fig. 7C) across multiple brain regions; scAAV9 consistently outperformed ssAAV9 in all histopathological assessments.

Nevertheless, *St3gal5*$^{-/-}$*/B4galnt1*$^{-/-}$ mice that survived after scAAV9-ST3GAL5.v2 treatment continued to exhibit hindlimb clasping, a sign of motor dysfunction not seen in their *St3gal5*$^{+/-}$*/B4galnt1*$^{-/-}$ littermates (Fig. 6H). This might reveal a fundamental limitation of the 'sequential double knockout' animal model; i.e., isolated knockout of *B4galnt1* in mice has independent neuropathological effects (*39, 40*) that cannot be fully rescued by replacing *ST3GAL5* alone. To test this hypothesis, we generated ssAAV9-CB-B4GALNT1 and co-delivered it with scAAV9-ST3GAL5.v2 by ICV administration. Indeed, this dual vector treatment regimen completely rescued lethality, growth retardation, hindlimb clasping, and motor impairment in *St3gal5*$^{-/-}$*/B4galnt1*$^{-/-}$ mice (Fig. 8). These encouraging results suggest that using the *St3gal5*$^{-/-}$*/B4galnt1*$^{-/-}$ mouse model to test *ST3GAL5* gene replacement may be overly stringent, and underrepresent the clinical potential of scAAV9 *ST3GAL5* gene replacement vectors.

IV injection of rAAV.PHP.eB-ST3GAL5.v2 improved phenotypic abnormalities in GM3SD mouse models

To examine whether systemically delivered scAAV9-ST3GAL5.v2 could achieve broader brain transduction and better therapeutic efficacy without causing liver toxicity, we treated *St3gal5*$^{-/-}$*/B4galnt1*$^{-/-}$ pups with 3x10^{11} gc on P1 by facial vein injection. Although we did not observe the acute lethality associated with systemic administration of first-generation vectors, intravenous scAAV9-ST3GAL5.v2 showed limited efficacy with regard to survival (median survival: 34 days), growth, and motor function (**Fig. S8B-D**), likely due to low *ST3GAL5* expression and poor ganglioside reconstitution in the brain as compared to ICV injection (**Fig. S8E-F**). We thus packaged the v2 construct into PHP.eB, an engineered AAV capsid that penetrates the murine blood-brain barrier more efficiently than AAV9 (*41*). Under the same systemic administration regimen, rAAV.PHP.eB-ST3GAL5.v2 led to higher transgene expression in the brain, robust CNS ganglioside restoration, and better phenotypic rescue by all measurements (**Fig. S8B-F**). Furthermore, co-delivery of rAAV.PHP.eB-ST3GAL5.v2 and rAAV.PHP.eB-CB-B4GALNT1 completely rescued hindlimb clasping and motor impairment in *St3gal5*$^{-/-}$*/B4galnt1*$^{-/-}$ mice (**Fig. S8G-H**). Taken together, these data underscore the importance of restoring ganglioside synthesis in CNS, particularly in neurons, for ameliorating the GM3SD phenotype.

Discussion

In this proof-of-concept study, we show that rAAV-mediated *ST3GAL5* gene replacement restores cerebral ganglioside synthesis, ameliorates neuropathology, and improves motor function in two different murine models of human GM3SD (*St3gal5*$^{-/-}$ and *St3gal5*$^{-/-}$*/B4galnt1*$^{-/-}$*)*. Of note, both ICV and IV routes of

administration provided clinically meaningful benefits in animal models, illustrating that CNS-directed *ST3GAL5* replacement holds promise for treating GM3SD patients.

Developmental and functional differences in ganglioside biology of mice as compared to humans present a significant experimental challenge. Humans with severe, biallelic loss-of-function mutations in *ST3GAL5* exhibit complete absence of GM3 and its downstream derivatives in plasma and presumably brain tissue, and present with epileptic encephalopathy and psychomotor stagnation within a few months of life. A similar enzyme disruption in *St3gal5*$^{-/-}$ mice leads to tissue deficiency of GM3 but a comparatively mild pathological and behavioral phenotype. A more phenotypically relevant murine model requires simultaneous disruption of two serial enzymes in the ganglioside synthetic pathway, *St3gal5* and *B4galnt1*. These double knockout mice exhibit severe neuropathology and functional deficits concordant with human GM3SD, but suffer from abiding and functionally relevant B4GALNT1 deficiency after successful ST3GAL5 replacement. Thus, while *St3gal5*$^{-/-}$*/B4galnt1*$^{-/-}$ mice allow us to test the efficacy of different *ST3GAL5* replacement vectors, they may underestimate the therapeutic potential of such vectors for treatment of human GM3SD. This scenario underscores the importance of using relevant animal models in preclinical gene therapy studies. Modeling GM3SD in larger gyrencephalic species, such as pigs or sheep, might prove more informative for future studies (*42*).

A number of other technical hurdles exist for the treatment of neurological diseases via gene replacement. For example, it is increasingly clear that for many neurogenetic deficiencies, successful treatment will depend on efficient and even delivery of transgene across the neuraxis coupled to a pattern of expression that approximates the natural distribution, abundance, and developmental timing of wild type protein. As an example, our first-generation vector induced an active unfolded protein response and severe hepatoxicity caused by off-target hepatic overexpression of ST3GAL5. Organ toxicity caused by transgene overexpression has been observed in other preclinical disease models. For example, mice administered AAV9-*MECP2* replacement vectors develop fatal liver disease associated with overabundant expression of MECP2 and its downstream mediators (*43*). In another murine system, long-term AAV9-mediated SMN overexpression triggers dose-dependent motor dysfunction, impaired proprioception, and neurodegenerative changes (*44*).

Towards safer and more efficacious therapy, we combined a neuron-specific human Syn1 promoter with a liver-specific miR122 targeting sequence in our second-generation vector. This design prevented ST3GAL5 overexpression in liver and thereby eliminated liver toxicity. The same principle of using facilitative cell-specific promoters coupled to inhibitory miRNA binding sites could be applied more broadly for achieving refined expression specificity (*45–47*). In general, we believe that optimizing spatial and temporal regulation of transgene expression will enable safer and more effective systemic gene therapy for a number of neurogenetic disorders in humans, and GM3SD provides an important experimental model to test this idea.

Lastly, to identify the most effective and clinically translatable route for administering *ST3GAL5* to CNS cells, we tested both ICV and IV routes commonly employed in current clinical trials (*48*).

Intracerebroventricular injection bypasses the BBB, similar in principle to the more spatially delimited intrathecal injection of nusinersen (*49*), but does not leverage the dense cytological distribution of natural CNS capillaries. We found that ICV delivery of *ST3GAL5* at a clinically feasible dose ($2x10^{13}$gc/kg) achieved promising therapeutic outcomes in neonatal mice. In contrast, IV injection vector at a 10-fold higher dose ($2x10^{14}$gc/kg) did not restore ganglioside production or prevent disease manifestations. Thus, among these preclinical dosing paradigms, ICV injection appeared superior at a clinically feasible dose.

Highly neurotropic AAV capsids, delivered systemically via CNS capillaries, may be key to achieving much broader CNS distribution. As a proof-of-concept, we tested IV delivery of *ST3GAL5* encapsulated in PHP.eB, an engineered capsid that crosses the murine BBB more efficiently than AAV9. The biochemical and phenotypic results were promising. Systemic delivery of PHP.eB is not clinically translatable, due to its species- and strain-specific characteristics, but our results can inform future studies of CNS favorable capsids.

In conclusion, AAV-mediated CNS gene transfer with *ST3GAL5* at a clinically relevant dose provides significant biochemical and therapeutic benefits with limited off-target toxicity. Notwithstanding limitations of current murine models, our second-generation scAAV9-ST3GAL5.v2 replacement vector is a promising candidate for translation to human trials.

Materials And Methods

Study design

The primary goal of this study was to develop a recombinant adeno-associated virus (rAAV)-mediated *ST3GAL5* replacement therapy to treat GM3 synthase deficiency (GM3SD). Our experimental approach combined GM3SD patient derived cells and mouse models to evaluate safety, efficacy, and duration of effect. Molecular and physiological readouts include delivery of rAAV genome, *ST3GAL5* expression, restoration of gangliosides, body and brain weight, motor functions, and survival. For each experiment, sample size reflected the number of independent biological replicates and was provided in the figure legends. Mice were assigned randomly to the experimental or control groups. Data from all animals were included in the analysis with no excluded outlier.

HeLa cell culture and transfection

HeLa cells were maintained in Dulbecco's Modified Eagle Medium, GlutaMAX Supplement (Gibco, Cat. No. 10569-010), supplemented with 10% (v/v) fetal bovine serum (Sigma, Cat. No. F2442) and antibiotics Penicillin-Streptomycin (100 U/ml) (Gibco, Cat. No. 15140-122) at 37°C with 5% CO_2. HeLa cells were transfected with Lipofectamine 3000 Transfection Reagent (Invitrogen, Cat. No. L3000015).

Induced pluripotent stem cell (iPSC) culture and differentiation

iPSCs were maintained in mTESR1 (STEMCELL Technologies, Cat. No. 85850), cultured in plates pre-coated with Matrigel (Corning, Cat. No. 354277), and passaged with Rho kinase inhibitor (Abcam, Cat. No. Ab120129). The cortical neuron differentiation was described in Shi et al (*50*). Briefly, iPSCs were cultured in neural maintenance media [DMEM:F12 + glutamax (Fisher Scientific, Cat. No. 10565018) and Neurobasal (Thermo Fisher Scientific, Cat. No. 21103049)], and firstly induced by neural induction media containing SB431542 (Tocris, Cat. No. 1614) and Dorsomorphin (Tocris, Cat. No. 3093) for 12 days to form the neuro-epithelial sheet. Then cells were passaged with dispase (Thermo Fisher Scientific, Cat. No. 17105041) to wells coated with laminin (Sigma-Aldrich, Cat. No. L2020) in neural maintenance medium. Cells were passaged and plated until post differentiation day 35 in the final plates pre-coated with poly-L-lysine (Sigma-Aldrich, Cat. No. P5899). Neurons were infected with lentiviral vectors in the presence of 8 μg/ml polybrene (Sigma-Aldrich, Cat. No. TR-1003-G).

Lentiviral vectors

Human *ST3GAL5* cDNA isoforms driven by cytomegalovirus-enhancer/chicken beta-actin promoter were cloned into the lentiviral transfer plasmid pLenti-CSCGW2. The 3rd generation system was used to package lentiviral vectors (*51*). Lentivirus vector plasmid was co-transfected with packaging genome plasmids (pMDLg/Prre and pRSV/REV) and envelope plasmid (pHCMV/VSVG) to HEK293T cells using $CaCl_2$ method. Lentivirus vector supernatants were harvested at 48h and 72h post-transfection and high-titer virus was concentrated via ultra-centrifugation. Virus titer was determined using QuickTiter™ Lentivirus Titer Kit (CELL BIOLABS, INC. Cat. No. VPK-107).

Western blot

Cell culture was lysed in ice-cold RIPA Lysis and Extraction Buffer (Thermo Fisher Scientific, Cat. No.89901) with cOmplete, EDTA-free protease inhibitor cocktail (Roche, Cat. No. 4693159001). Cell lysate was then sonicated. Debris was removed by centrifugation (10 minutes, 13,000 rpm, 4°C) and supernatant was collected. Total protein concentration was determined using Bicinchoninic Acid (BCA) protein assay kit (Thermo Fisher Scientific, Cat. No. 23252). Lysates containing equal amount of total protein were boiled in Tris-Glycine SDS Sample Buffer (Invitrogen, Cat. No. LC2676) at 95°C for 5 min. Primary antibodies rabbit anti-ST3GAL5 (Thermo Fisher Scientific, Cat. No. PA5-25730, 1:1,000 dilution), mouse anti-actin (Abcam, Cat. No. ab8226, 1:5,000 dilution) and secondary antibodies IRDye 680RD Donkey anti-Rabbit IgG (LI-COR Biosciences, Cat. No. 926-68073, 1:5,000 dilution), IRDye 800CW Donkey anti-Mouse IgG (LI-COR Biosciences, Cat. No. 926-32212, 1:5,000 dilution) were applied in Western blot. Membrane was scanned with a LI-COR Odyssey scanner (LI-COR).

Immunofluorescence (IF) staining

IF was performed in iPSC-derived cortical neurons and mouse brain sections. Cortical neurons were fixed with 4% paraformaldehyde (Electron Microscopy Sciences, Cat. No. 15710) after washing with Dulbecco's Phosphate-Buffered Saline (DPBS) (Thermo Fisher Scientific, Cat. No. 14190144). Following that, cells were permeabilized with 0.2% (vol/vol) Triton x-100 for neural markers or not for gangliosides staining and blocked with 5% goat serum (Invitrogen, Cat. No. 50062Z) in 0.2% (vol/vol) Triton x-100. Mouse brain

was fixed in 4% paraformaldehyde at 4°C overnight. The next day, brains were soaked in 30% sucrose at 4°C overnight until balanced. Brains were then mounted in O.C.T. compound (Midland Scientific, Cat. No. SAKURA 4583) and stored at -80°C until cryo-sectioning. Brain slices were permeabilized with 0.5% (vol/vol) Triton x-100 and blocked with 5% goat serum (Invitrogen, Cat. No. 50062Z). Primary antibodies, chicken anti-microtubule-associated protein 2 (MAP2) (Abcam, Cat. No. ab5392, 1:1,000 dilution), mouse anti-beta III Tubulin (Tuj1) (Abcam, Cat. No. ab78078, 1:1,000 dilution), rat anti-COUP-IF-interacting protein 2 (Ctip2) (Abcam, Cat. No. ab18465, 1:500 dilution), rabbit anti-T-box brain transcription factor 1 (Tbr1) (Abcam, Cat. No. ab31940, 1:1,000 dilution), mouse anti-ganglioside GD1a (DSHB, Cat. No. GD1a-1, 1:100 dilution), mouse anti-ganglioside GD1b (DSHB, Cat. No. GD1b01, 1:100 dilution), and mouse anti-ganglioside GT1b (DSHB, Cat. No. GT1b-1, 1:100 dilution) were used in immunodetection in blocking buffer at 4°C overnight. Secondary antibodies goat anti-chicken IgY H&L, Alexa Fluor 488 (Abcam, Cat. No. ab150169, 1:1,000 dilution), donkey anti-mouse IgG H&L, Alexa Fluor 594 (Abcam, Cat. No. ab150108, 1:1,000 dilution), goat anti-rat IgG H&L, Alexa Fluor 647 (Abcam, Cat. No. ab150167, 1:1,000 dilution), goat anti-rabbit IgG H&L, Alexa Fluor 488 (Abcam, Cat. No. ab150077, 1:1,000 dilution) and goat anti-mouse IgG H&L, Alexa Fluor 488 (Thermo Fisher, Cat. No. A11029) were incubated within blocking buffer at room temperature for one hour. Sliced were mounted using Prolong Diamond Antifade Mountant with DAPI (Fisher scientific, Cat. No. P36962). Images were taken on a Leica TCS SP8 confocal microscope. Quantification of GD1a and GD1b was performed using the ImageJ software.

Adeno-associated virus (AAV) vectors

Human *ST3GAL5* cDNA isoforms driven by cytomegalovirus-enhancer/chicken beta-actin promoter and human *ST3GAL5* cDNA isoforms plus miR122 binding sites driven by Synapsin1 promoter were cloned into AAV plasmids. The plasmids were sequenced throughout the expression cassette, and the integrity of inverted terminal repeats (ITR) was confirmed by restriction enzyme digestion. AAV vectors were produced by transient triple transfection in HEK293 cells and purified by CsCl gradient sedimentation for AAV9 or by iodixanol gradient sedimentation for PHP.eB vectors. Vector titers were determined by droplet digital PCR and vector purity was assessed by gel electrophoresis followed by silver staining.

Animal use

All animal procedures were reviewed and approved by The Institutional Animal Care and Use Committee (IACUC) at University of Massachusetts Chan Medical School and performed in compliance with all relevant ethical regulations. St3gal5$^{-/-}$/B4galnt1$^{+/-}$ males were imported from Regeneron Pharmaceuticals, Inc. and bred with C57BL6NTac female (TACONIC, B6-F). Newborns were genotyped at the date of birth. Briefly, 1mm tail tips were cut. Genomic DNA was extracted by boiling in 25mM NaOH + 0.4mM EDTA (pH 8.0) at 100°C for 90 minutes, followed by mixing with 40mM Tris-Hcl (pH 8.0). *St3gal5* and *B4galnt1* genes were determined by quantitative PCR (qPCR) using Taqman reagents targeting *St3gal5* (Thermo Fisher Scientific, Assay ID: APH6DZ6, 9057mTGU; Assay ID: APMFZ6Z, 9057mTGD), *B4galnt1* (LGC Biosearch Technologies, Cat. No. DLOM-RFB-5, Assay ID: 15582TU; Assay ID: LacZ) and *Tfrc* (Thermo Fisher Scientific, Cat. No. 4458367). Primer and probe sequences can be found in **Table S1**. To harvest tissues, mice were anesthetized with isoflurane and transcardially perfused with ice-cold PBS.

Tissues were immediately dissected, snap-frozen in liquid nitrogen, and stored at -80°C. Facial vein injections were performed on postnatal day 1 (P1) via right facial vein at $3x10^{11}$ genome copies (GC) per pup. Intracerebroventricular (I.C.V.) injections were performed on P1 at $3x10^{10}$ GC bilaterally per pup. After procedure, pups were cleaned with 70% ethanol and rubbed with bedding material.

DNA/RNA extraction, quantitative Realtime PCR (qPCR) and droplet digital PCR (ddPCR)

Total DNA and RNA were extracted from snap frozen mouse tissues using AllPrep DNA/RNA Mini kit (Qiagen, Cat. No. 80204). Viral vector genome copy number was determined in a multiplexed reaction using ddPCR Supermix for Probes (No dUTP) (Bio-Rad, Cat. No. 1863024) and Taqman reagents targeting *ST3GAL5* (Thermo Fisher Scientific, Assay ID: APGZHGD) and *Tfrc* (Thermo Fisher Scientific, Cat. No. 4458367). One µg of total RNA was reverse transcribed into cDNA using High-capacity cDNA Reverse Transcription Kit (Applied Biosystems, Cat. No. 4368813). Exogenous human *ST3GAL5* and mouse *St3gal5* cDNA were quantified in a multiplexed reaction using Taqman reagents targeting *ST3GAL5* (Thermo Fisher Scientific, Assay ID: APGZHGD), *St3gal5* (Thermo Fisher Scientific, Assay ID: Mm00488232_m1) and *Gusb* (Thermo Fisher Scientific, Assay ID: Mm01197698_m1). ddPCR was performed with a QX200 ddPCR system (Bio-Rad). qPCR was performed on a ViiA 7 Real-Time PCR system using Taqman Gene expression master mix (Thermo Fisher Scientific, Cat. No. 4369016) and Taqman reagents targeting *Chop* (Thermo Fisher Scientific, Assay ID: Mm01135937_g1) and *Tnfa* (Thermo Fisher Scientific, Assay ID: Mm00443260_g1).

Mass spectrometry (MS)

Brain tissue samples were homogenized in water (4 mL/g wet tissue) using an Omni Bead Ruptor (Cole-Parmer, Cat No. Mfr19-628). The LacCer, GM1, GM2, GM3 were extracted from 50uL of homogenate or serum with 200uL of methanol containing d3-Lc (16:0) (Matreya LLC, Cat. No, 1534), d3-GM1 (18:0) (Matreya LLC, Cat. No. 2050), d3-GM2 (18:0) (Matreya LLC, Cat. No, 2051), and d3-GM3 (18:0) (Matreya LLC, Cat. No. 2052) as the internal standards for LacCer, GM1, GM2, GM3, respectively. Quality control (QC) samples were prepared by pooling aliquots of positive samples and injected every five study samples to monitor instrument performance throughout these analyses. The analysis of LacCer, GM1, GM2, GM3 was performed on a Shimadzu 20AD HPLC system and a SIL-20AC autosampler coupled to 6500QTRAP + mass spectrometer (AB Sciex) operated in positive multiple reaction monitoring mode. Data processing was conducted with Analyst 1.6.3 (Applied Biosystems). The relative quantification data for all analytes were presented as the peak ratios of analytes to their internal standard.

Mouse monitoring and behavioral assays

Mice were blindly weighed every other day until weaning at 21 days old. After weaning, each mouse was weighed and evaluated weekly by a trained observer for adverse events.

Negative geotaxis

Negative geotaxis assay was examined every other day for P9-P15 pups on a 45° incline plane. Prior to the test, animals were placed on the plane to acclimate for one minute. Mouse head was facing downwards, success was marked when mouse rotated 180° to the head-up position while failure was when mouse dropped off from the plane. The ability of finishing the assay was recorded. Each mouse was tested for three times and the success rate of completing the assay was plotted.

Accelerated rotarod

Coordinated motor functions were examined in treated mice and littermates using the 4-40rpm accelerating rotarod test. Mice were tested at six weeks old and ten weeks old. Tested mice were trained two days before the testing day for three tests each. Prior to the test, the animals were placed on the rotarod machine to acclimate for at least one minute. Each mouse was tested for three times and the best latency to fall was recorded and plotted.

Histology and immunohistochemistry (IHC)

Mouse brain and liver were fixed in 10% formalin (Fisher Scientific, Cat. No. SF100-20). Paraffin embedding, sectioning, hematoxylin and eosin (H&E) staining, terminal deoxynucleotidyl transferase dUTP nick end labelling (TUNEL) staining (Roche, Cat. No. 11684817910) and IHC were performed by the Morphology Core at University of Massachusetts Chan Medical School under standard conditions. Mouse anti-GFAP antibody (EMD Millipore, Cat. No. MAB360, 1:500 dilution) was used in IHC. Images were taken on a Leica DM5500 B microscope. The quantification of GFAP IHC was performed using the Image FIJI software as previously described (*52*).

ProcartaPlex multiplex immunoassays

Total protein was extracted in ice-cold RIPA Lysis and Extraction Buffer (Thermo Fisher Scientific, Cat. No.89901) with cOmplete, EDTA-free protease inhibitor cocktail (Roche, Cat. No. 4693159001) from snap frozen tissues. Protein concentration was determined using Bicinchoninic Acid (BCA) protein assay kit (Thermo Fisher Scientific, Cat. No. 23252). Normalized protein extracts were loaded on procartaplex mix&match panel (Thermo Fisher Scientific). Values were acquired by Bio-Plex MAGPIX (Bio-Rad).

Messenger RNA sequencing (RNA-seq)

RNA-seq was carried out by Novegene (Novogene Corporation Inc, CA) under standard conditions. RNA was extracted using Trizol phase separation method from cell debris. Isolated RNA sample integrity and concentration was assessed by Agilent bioanalyzer 2100. A total amount of 1 μg RNA per sample was used as input material for RNA sample preparations. Sequencing libraries were generated using NEBNext® Ultra RNA Library Prep Kit for Illumina® (New England BioLabs, Cat. No. E7770L) following manufacturer's recommendations. Briefly, mRNA was purified from total RNA using poly-T oligo-attached magnetic beads. Fragmentation was carried out using divalent cations under elevated temperature in NEBNext First Strand Synthesis Reaction Buffer (5X) (New England BioLabs). First strand cDNA was synthesized using random hexamer primer and M-MuL V Reverse Transcriptase (RNase H-). Second strand cDNA synthesis was subsequently performed using DNA Polymerase I and RNase H. Final libraries

quantity was assessed on the Agilent Bioanalyzer 2100 system. The clustering of the index-coded samples were performed on a cBot Cluster Generation System using PEE Cluster Kit cBot-HS (Illumina, California, USA) according to the manufacturer's instructions. After cluster generation, the library preparations were sequenced on an Illumina NovaSeq 6000 platform and paired-end reads were generated.

For data analysis, 3' adapter sequence was removed using Trimmomatic (with parameters ILLUMINACLIP, min_length, 10; seed mismatches, 2; palindrome clip threshold, 30; simple clip threshold, 5). Then, reads were mapped to mouse_mm10_gencode_ using STAR. To estimate expression levels, RSEM55 was used to align reads to a predefined set of transcripts from GENCODE. Finally, the RSEM quantification matrix, i.e., estimated counts for each gene and/or for each annotated isoform, was used for differential gene expression analysis. Count matrix was loaded into DEBrowser software for interactive analysis. Data analysis was performed on the RNA-seq pipeline of the DolphinNext (*53*).

Statistical analysis

All data are presented as mean ± SD and analyzed using GraphPad Prism software (Version 9). Two-sided student t-test was used to compare two groups, and one-way analysis of variance (ANOVA) was used to compare among multiple groups. Animal weight was analyzed by two-way ANOVA and survival was analyzed by Log-rank (Mantel-Cox) test. *p < 0.05, **p < 0.01, ***p < 0.001, ****p < 0.0001, ns: not significant.

Declarations

Acknowledgements: We wish to thank M. Dookwah and M. Tiemeyer for providing patient iPSCs. We thank Regeneron Pharmaceuticals, Inc. for providing *St3gal5/B4galnt1* mouse. We thank X. Jiang for performing MS and analysis. We are very grateful to the Gao lab, Viral Vector Core, Clinic for Special Children, the Animal Medicine and DERC Morphology Cores and X. Li for advice, technical support, and manuscript review.

Funding: G.G. is supported by grants from the University of Massachusetts Medical School (an internal grant), by the NIH (R01NS076991-01, P01HL131471-05, R01AI121135, UG3HL147367-01, R01HL097088, R01HL152723-02, U19AI149646-01, and UH3HL147367-04).

Author contributions: GG and KAS conceived project; HY, DW, KAS, GG designed experimental plan; HY performed cell, animal, and mouse tissue experiments; HY analyzed data with critical input from RHB, DW and GG; HY, DW, and GG wrote manuscript; KAS and GG supervised project.

Competing interests: GG is a scientific cofounder of Voyager Therapeutics, Adrenas Therapeutics, and Aspa Therapeutics, and holds equity in these companies. GG is an inventor on patents with potential royalties licensed to Voyager Therapeutics, Aspa Therapeutics, and ten other biopharmaceutical companies. The remaining authors declare no competing interests.

Data and materials availability: mRNA-seq data can be found in thee NCBI's Gene Expression Omnibus (GEO) using GEO series accession number GSE201587. Other data supporting the findings of this study are available within the paper, or from the corresponding authors upon reasonable request.

References

1. M. A. Simpson, H. Cross, C. Proukakis, D. A. Priestman, D. C. Neville, G. Reinkensmeier, H. Wang, M. Wiznitzer, K. Gurtz, A. Verganelaki, A. Pryde, M. A. Patton, R. A. Dwek, T. D. Butters, F. M. Platt, A. H. Crosby, Infantile-onset symptomatic epilepsy syndrome caused by a homozygous loss-of-function mutation of GM3 synthase. *Nat Genet* **36**, 1225-1229 (2004).

2. J. S. Lee, Y. Yoo, B. C. Lim, K. J. Kim, J. Song, M. Choi, J. H. Chae, GM3 synthase deficiency due to ST3GAL5 variants in two Korean female siblings: Masquerading as Rett syndrome-like phenotype. *Am J Med Genet A* **170**, 2200-2205 (2016).

3. L. E. Bowser, M. Young, O. K. Wenger, Z. Ammous, K. W. Brigatti, V. J. Carson, T. Moser, J. Deline, K. Aoki, T. Morlet, E. M. Scott, E. G. Puffenberger, D. L. Robinson, C. Hendrickson, J. Salvin, S. Gottlieb, A. D. Heaps, M. Tiemeyer, K. A. Strauss, Recessive GM3 synthase deficiency: Natural history, biochemistry, and therapeutic frontier. *Mol Genet Metab*, (2019).

4. K. Fragaki, S. Ait-El-Mkadem, A. Chaussenot, C. Gire, R. Mengual, L. Bonesso, M. Beneteau, J. E. Ricci, V. Desquiret-Dumas, V. Procaccio, A. Rotig, V. Paquis-Flucklinger, Refractory epilepsy and mitochondrial dysfunction due to GM3 synthase deficiency. *Eur J Hum Genet* **21**, 528-534 (2013).

5. H. Wang, A. Bright, B. Xin, J. R. Bockoven, A. S. Paller, Cutaneous dyspigmentation in patients with ganglioside GM3 synthase deficiency. *Am J Med Genet A* **161A**, 875-879 (2013).

6. P. H. Fishman, S. R. Max, J. F. Tallman, R. O. Brady, N. K. Maclaren, M. Cornblath, Deficient Ganglioside Biosynthesis: a novel human sphingolipidosis. *Science* **187**, 68-70 (1975).

7. L. Boccuto, K. Aoki, H. Flanagan-Steet, C. F. Chen, X. Fan, F. Bartel, M. Petukh, A. Pittman, R. Saul, A. Chaubey, E. Alexov, M. Tiemeyer, R. Steet, C. E. Schwartz, A mutation in a ganglioside biosynthetic enzyme, ST3GAL5, results in salt & pepper syndrome, a neurocutaneous disorder with altered glycolipid and glycoprotein glycosylation. *Hum Mol Genet* **23**, 418-433 (2014).

8. R. L. Schnaar, Glycolipid-mediated cell-cell recognition in inflammation and nerve regeneration. *Arch Biochem Biophys* **426**, 163-172 (2004).

9. L. Mayo, S. A. Trauger, M. Blain, M. Nadeau, B. Patel, J. I. Alvarez, I. D. Mascanfroni, A. Yeste, P. Kivisakk, K. Kallas, B. Ellezam, R. Bakshi, A. Prat, J. P. Antel, H. L. Weiner, F. J. Quintana, Regulation of astrocyte activation by glycolipids drives chronic CNS inflammation. *Nat Med* **20**, 1147-1156 (2014).

10. H. Wang, V. Sency, P. McJarrow, A. Bright, Q. Huang, K. Cechner, J. Szekely, J. Brace, A. Wang, D. Liu, A. Rowan, M. Wiznitzer, A. Zhou, B. Xin, Oral Ganglioside Supplement Improves Growth and Development in Patients with Ganglioside GM3 Synthase Deficiency. *JIMD Rep* **45**, 9-20 (2019).

11. T. Yamashita, A. Hashiramoto, M. Haluzik, H. Mizukami, S. Beck, A. Norton, M. Kono, S. Tsuji, J. L. Daniotti, N. Werth, R. Sandhoff, K. Sandhoff, R. L. Proia, Enhanced insulin sensitivity in mice lacking ganglioside GM3. *Proc Natl Acad Sci U S A* **100**, 3445-3449 (2003).

12. M. Yoshikawa, S. Go, K. Takasaki, Y. Kakazu, M. Ohashi, M. Nagafuku, K. Kabayama, J. Sekimoto, S. Suzuki, K. Takaiwa, T. Kimitsuki, N. Matsumoto, S. Komune, D. Kamei, M. Saito, M. Fujiwara, K. Iwasaki, J. Inokuchi, Mice lacking ganglioside GM3 synthase exhibit complete hearing loss due to selective degeneration of the organ of Corti. *Proc Natl Acad Sci U S A* **106**, 9483-9488 (2009).

13. T. Yamashita, Y. P. Wu, R. Sandhoff, N. Werth, H. Mizukami, J. M. Ellis, J. L. Dupree, R. Geyer, K. Sandhoff, R. L. Proia, Interruption of ganglioside synthesis produces central nervous system degeneration and altered axon-glial interactions. *Proc Natl Acad Sci U S A* **102**, 2725-2730 (2005).

14. H. Yang, R. H. Brown, Jr., D. Wang, K. A. Strauss, G. Gao, AAV-Mediated Gene Therapy for Glycosphingolipid Biosynthesis Deficiencies. *Trends Mol Med* **27**, 520-523 (2021).

15. D. Wang, P. W. L. Tai, G. Gao, Adeno-associated virus vector as a platform for gene therapy delivery. *Nat Rev Drug Discov*, (2019).

16. D. F. Aschauer, S. Kreuz, S. Rumpel, Analysis of transduction efficiency, tropism and axonal transport of AAV serotypes 1, 2, 5, 6, 8 and 9 in the mouse brain. *PLoS One* **8**, e76310 (2013).

17. C. N. Mattar, S. N. Waddington, A. Biswas, N. Johana, X. W. Ng, A. S. Fisk, N. M. Fisk, L. G. Tan, A. A. Rahim, S. M. Buckley, M. H. Tan, J. Lu, M. Choolani, J. K. Chan, Systemic delivery of scAAV9 in fetal macaques facilitates neuronal transduction of the central and peripheral nervous systems. *Gene Ther* **20**, 69-83 (2013).

18. D. Chand, F. Mohr, H. McMillan, F. F. Tukov, K. Montgomery, A. Kleyn, R. Sun, S. Tauscher-Wisniewski, P. Kaufmann, G. Kullak-Ublick, Hepatotoxicity following administration of onasemnogene abeparvovec (AVXS-101) for the treatment of spinal muscular atrophy. *J Hepatol* **74**, 560-566 (2021).

19. C. Hinderer, N. Katz, E. L. Buza, C. Dyer, T. Goode, P. Bell, L. K. Richman, J. M. Wilson, Severe Toxicity in Nonhuman Primates and Piglets Following High-Dose Intravenous Administration of an Adeno-Associated Virus Vector Expressing Human SMN. *Hum Gene Ther* **29**, 285-298 (2018).

20. L. Morales, Y. Gambhir, J. Bennett, H. H. Stedman, Broader Implications of Progressive Liver Dysfunction and Lethal Sepsis in Two Boys following Systemic High-Dose AAV. *Mol Ther* **28**, 1753-1755 (2020).

21. High-dose AAV gene therapy deaths. *Nat Biotechnol* **38**, 910 (2020).

22. J. Xie, Q. Xie, H. Zhang, S. L. Ameres, J. H. Hung, Q. Su, R. He, X. Mu, S. Seher Ahmed, S. Park, H. Kato, C. Li, C. Mueller, C. C. Mello, Z. Weng, T. R. Flotte, P. D. Zamore, G. Gao, MicroRNA-regulated, systemically delivered rAAV9: a step closer to CNS-restricted transgene expression. *Mol Ther* **19**, 526-535 (2011).

23. C. Qiao, Z. Yuan, J. Li, B. He, H. Zheng, C. Mayer, J. Li, X. Xiao, Liver-specific microRNA-122 target sequences incorporated in AAV vectors efficiently inhibits transgene expression in the liver. *Gene Ther* **18**, 403-410 (2011).

24. S. Uemura, S. Yoshida, F. Shishido, J. Inokuchi, The cytoplasmic tail of GM3 synthase defines its subcellular localization, stability, and in vivo activity. *Mol Biol Cell* **20**, 3088-3100 (2009).

25. P. Berselli, S. Zava, E. Sottocornola, S. Milani, B. Berra, I. Colombo, Human GM3 synthase: a new mRNA variant encodes an NH2-terminal extended form of the protein. *Biochim Biophys Acta* **1759**, 348-358 (2006).

26. K. W. Kim, S. W. Kim, K. S. Min, C. H. Kim, Y. C. Lee, Genomic structure of human GM3 synthase gene (hST3Gal V) and identification of mRNA isoforms in the 5'-untranslated region. *Gene* **273**, 163-171 (2001).

27. M. Kozak, Pushing the limits of the scanning mechanism for initiation of translation. *Gene* **299**, 1-34 (2002).

28. J. I. Inokuchi, K. I. Inamori, K. Kabayama, M. Nagafuku, S. Uemura, S. Go, A. Suzuki, I. Ohno, H. Kanoh, F. Shishido, Biology of GM3 Ganglioside. *Prog Mol Biol Transl Sci* **156**, 151-195 (2018).

29. S. Ngamukote, M. Yanagisawa, T. Ariga, S. Ando, R. K. Yu, Developmental changes of glycosphingolipids and expression of glycogenes in mouse brains. *J Neurochem* **103**, 2327-2341 (2007).

30. S. Sipione, J. Monyror, D. Galleguillos, N. Steinberg, V. Kadam, Gangliosides in the Brain: Physiology, Pathophysiology and Therapeutic Applications. *Front Neurosci* **14**, 572965 (2020).

31. V. Coelho-Santos, A. A. Berthiaume, S. Ornelas, H. Stuhlmann, A. Y. Shih, Imaging the construction of capillary networks in the neonatal mouse brain. *Proc Natl Acad Sci U S A* **118**, (2021).

32. S. F. Tzeng, G. E. Deibler, G. H. DeVries, Myelin basic protein and myelin basic protein peptides induce the proliferation of Schwann cells via ganglioside GM1 and the FGF receptor. *Neurochem Res* **24**, 255-260 (1999).

33. K. Ogawa-Goto, N. Funamoto, Y. Ohta, T. Abe, K. Nagashima, Myelin gangliosides of human peripheral nervous system: an enrichment of GM1 in the motor nerve myelin isolated from cauda equina. *J Neurochem* **59**, 1844-1849 (1992).

34. L. Svennerholm, K. Bostrom, P. Fredman, B. Jungbjer, A. Lekman, J. E. Mansson, B. M. Rynmark, Gangliosides and allied glycosphingolipids in human peripheral nerve and spinal cord. *Biochim Biophys Acta* **1214**, 115-123 (1994).

35. K. Bey, C. Ciron, L. Dubreil, J. Deniaud, M. Ledevin, J. Cristini, V. Blouin, P. Aubourg, M. A. Colle, Efficient CNS targeting in adult mice by intrathecal infusion of single-stranded AAV9-GFP for gene therapy of neurological disorders. *Gene Ther* **24**, 325-332 (2017).

36. S. Kugler, E. Kilic, M. Bahr, Human synapsin 1 gene promoter confers highly neuron-specific long-term transgene expression from an adenoviral vector in the adult rat brain depending on the transduced area. *Gene Ther* **10**, 337-347 (2003).

37. Z. Wang, H. I. Ma, J. Li, L. Sun, J. Zhang, X. Xiao, Rapid and highly efficient transduction by double-stranded adeno-associated virus vectors in vitro and in vivo. *Gene Ther* **10**, 2105-2111 (2003).

38. D. M. McCarty, H. Fu, P. E. Monahan, C. E. Toulson, P. Naik, R. J. Samulski, Adeno-associated virus terminal repeat (TR) mutant generates self-complementary vectors to overcome the rate-limiting step to transduction in vivo. *Gene Ther* **10**, 2112-2118 (2003).

39. D. Yao, R. McGonigal, J. A. Barrie, J. Cappell, M. E. Cunningham, G. R. Meehan, S. N. Fewou, J. M. Edgar, E. Rowan, Y. Ohmi, K. Furukawa, K. Furukawa, P. J. Brophy, H. J. Willison, Neuronal expression of GalNAc transferase is sufficient to prevent the age-related neurodegenerative phenotype of complex ganglioside-deficient mice. *J Neurosci* **34**, 880-891 (2014).

40. K. A. Sheikh, J. Sun, Y. Liu, H. Kawai, T. O. Crawford, R. L. Proia, J. W. Griffin, R. L. Schnaar, Mice lacking complex gangliosides develop Wallerian degeneration and myelination defects. *Proc Natl Acad Sci U S A* **96**, 7532-7537 (1999).

41. K. Y. Chan, M. J. Jang, B. B. Yoo, A. Greenbaum, N. Ravi, W. L. Wu, L. Sanchez-Guardado, C. Lois, S. K. Mazmanian, B. E. Deverman, V. Gradinaru, Engineered AAVs for efficient noninvasive gene delivery to the central and peripheral nervous systems. *Nat Neurosci* **20**, 1172-1179 (2017).

42. M. Casal, M. Haskins, Large animal models and gene therapy. *Eur J Hum Genet* **14**, 266-272 (2006).

43. V. Matagne, E. Borloz, Y. Ehinger, L. Saidi, L. Villard, J. C. Roux, Severe offtarget effects following intravenous delivery of AAV9-MECP2 in a female mouse model of Rett syndrome. *Neurobiol Dis* **149**, 105235 (2021).

44. M. Van Alstyne, I. Tattoli, N. Delestree, Y. Recinos, E. Workman, L. S. Shihabuddin, C. Zhang, G. Z. Mentis, L. Pellizzoni, Gain of toxic function by long-term AAV9-mediated SMN overexpression in the sensorimotor circuit. *Nat Neurosci* **24**, 930-940 (2021).

45. A. Geisler, A. Jungmann, J. Kurreck, W. Poller, H. A. Katus, R. Vetter, H. Fechner, O. J. Muller, microRNA122-regulated transgene expression increases specificity of cardiac gene transfer upon intravenous delivery of AAV9 vectors. *Gene Ther* **18**, 199-209 (2011).

46. A. Majowicz, P. Maczuga, K. L. Kwikkers, S. van der Marel, R. van Logtenstein, H. Petry, S. J. van Deventer, P. Konstantinova, V. Ferreira, Mir-142-3p target sequences reduce transgene-directed immunogenicity following intramuscular adeno-associated virus 1 vector-mediated gene delivery. *J Gene Med* **15**, 219-232 (2013).

47. D. J. Gessler, D. Li, H. Xu, Q. Su, J. Sanmiguel, S. Tuncer, C. Moore, J. King, R. Matalon, G. Gao, Redirecting N-acetylaspartate metabolism in the central nervous system normalizes myelination and rescues Canavan disease. *JCI Insight* **2**, e90807 (2017).

48. E. Hudry, L. H. Vandenberghe, Therapeutic AAV Gene Transfer to the Nervous System: A Clinical Reality. *Neuron* **101**, 839-862 (2019).

49. E. Mercuri, B. T. Darras, C. A. Chiriboga, J. W. Day, C. Campbell, A. M. Connolly, S. T. Iannaccone, J. Kirschner, N. L. Kuntz, K. Saito, P. B. Shieh, M. Tulinius, E. S. Mazzone, J. Montes, K. M. Bishop, Q. Yang, R. Foster, S. Gheuens, C. F. Bennett, W. Farwell, E. Schneider, D. C. De Vivo, R. S. Finkel, C. S. Group, Nusinersen versus Sham Control in Later-Onset Spinal Muscular Atrophy. *N Engl J Med* **378**, 625-635 (2018).

50. Y. Shi, P. Kirwan, F. J. Livesey, Directed differentiation of human pluripotent stem cells to cerebral cortex neurons and neural networks. *Nat Protoc* **7**, 1836-1846 (2012).

51. M. Sena-Esteves, G. Gao, Production of High-Titer Retrovirus and Lentivirus Vectors. *Cold Spring Harb Protoc* **2018**, (2018).

52. A. R. Crowe, W. Yue, Semi-quantitative Determination of Protein Expression using Immunohistochemistry Staining and Analysis: An Integrated Protocol. *Bio Protoc* **9**, (2019).

53. O. Yukselen, O. Turkyilmaz, A. R. Ozturk, M. Garber, A. Kucukural, DolphinNext: a distributed data processing platform for high throughput genomics. *BMC Genomics* **21**, 310 (2020).

Figures

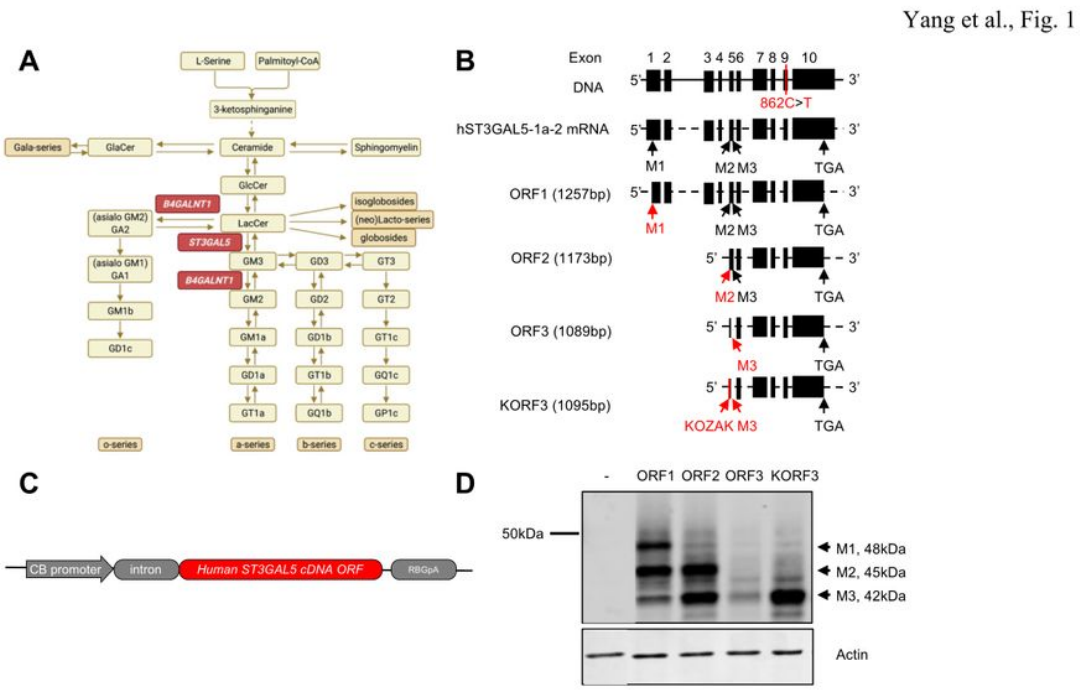

Figure 1

GM3 synthase deficiency is caused by loss-of-function mutation of *ST3GAL5*.

(**A**). Schematic showing *de novo* gangliosides synthesis pathway. ST3GAL5 uses lactosylceramide (LacCer) as substrate to synthesize GM3, the precursor of all other gangliosides. B4GALNT1 is another key enzyme to catalyze the complex gangliosides formation. Loss-of-function mutations in *ST3GAL5* and *B4GALNT1* cause GM3 synthase deficiency (GM3SD) and Hereditary Spastic Paraplegia Type 26 (HSP26), respectively. (**B**). Schematic of human *ST3GAL5* DNA genome and the most abundant mRNA isoform noted in NCBI (NM_003896). M1, M2, and M3 represent three initiating starting codon methionine. Stop codon TGA is at exon 10 and Amish mutation (p.862C>T) locates at exon 9. cDNA initiating from M1 (ORF1), M2 (ORF2), M3 (ORF3), and Kozak+M3 (KORF3) possesses 1257bp, 1173bp, 1089bp, and 1095bp size, respectively. Black boxes, exons; black lines, introns; dashed black lines, spliced

introns. (**C**). Construct expressing ubiquitous human *ST3GAL5* ORF is shown. (**D**). Representative Western blot images of ST3GAL5 protein expression via different ORF transfection in HeLa cell.

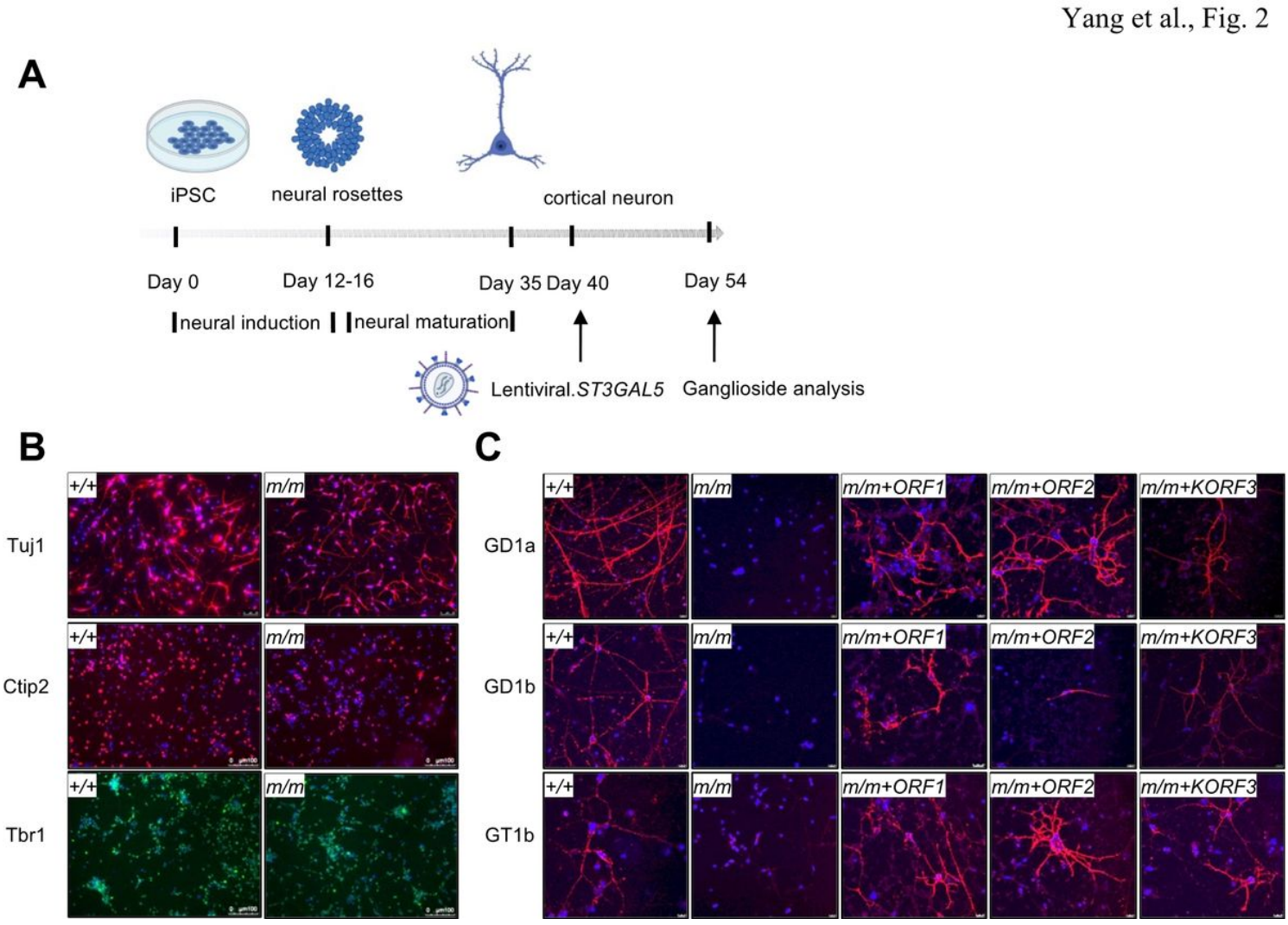

Figure 2

ST3GAL5 replacement restores gangliosides production in iPSC-derived cortical neurons.

(**A**). Workflow to examine restoration of gangliosides production in patient induced pluripotent stem cell (iPSC) differentiated cortical neurons by lentiviral vectors expressing *ST3GAL5* ORFs. (**B**). Representative images of neuronal markers in $ST3GAL5^{+/+}$ and $ST3GAL5^{mut/mut}$ iPSC differentiated cortical neurons. Neuron-specific class III beta-tubulin (Tuj1), red; COUP-TF-interacting protein 2 (Ctip2), red; T-Box Brain Transcription Factor 1 (TBR1), green; nuclei, counterstaining in blue. *+/+*, wildtype; *m/m*, $ST3GAL5^{mut/mut}$. (**C**). Representative images of major brain gangliosides in cortical neurons by lentiviral vectors expressing *ST3GAL5* ORFs. GD1a, GD1b, GT1b, red; nuclei, counterstaining in blue. *+/+*, wildtype; *m/m*, $ST3GAL5^{mut/mut}$.

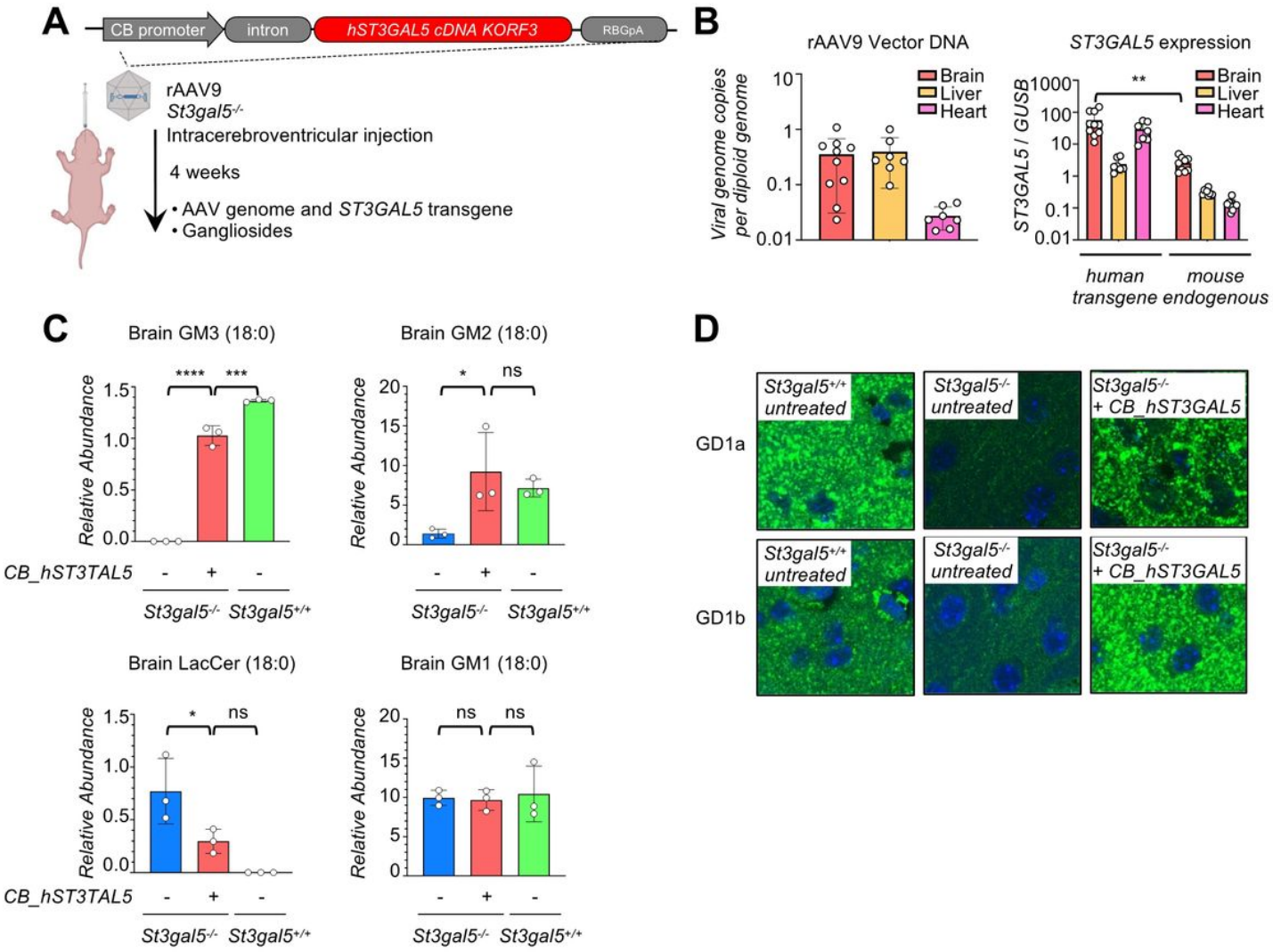

Figure 3

I.C.V. delivery of *ST3GAL5* restores gangliosides production in *St3gal5*$^{-/-}$ mouse model.

(**A**). Schematic of intracerebroventricular (I.C.V.) delivery of ubiquitous human *ST3GAL5* cDNA Kozak ORF3 (KORF3) in *St3gal5*$^{-/-}$ mouse model. (**B**). Droplet digital PCR (ddPCR) quantification of rAAV9 vector genome and human *ST3GAL5* transgene in the brain, liver, and heart of rAAV9.CB.hST3GAL5 treated *St3gal5*$^{-/-}$ mice. Mouse endogenous *St3gal5* mRNA was quantified from brain (Br), liver (Li), and heart (He) of *St3gal5*$^{+/+}$ mice. Data are mean ± s.d. of 7-10 animals per group. Statistical analysis was performed by t-test. **p<0.01. (**C**). Mass Spectrometry (MS) quantification of GM3 (18:0), GM2 (18:0), LacCer (18:0), and GM1 (18:0) from the brain of *St3gal5*$^{+/+}$ and *St3gal5*$^{-/-}$ mice, with (+) or without (-) rAAV9.CB.hST3GAL5 treatment. Data are mean ± s.d. of 3 animals per group. Statistical analysis was performed by one-way ANOVA, followed by Sidak's multiple comparisons test. *p<0.05, **p<0.01, ***p<0.001, ****p<0.0001, ns: not significant. (**D**). Representative images of major brain gangliosides in

cortex of *St3gal5*$^{+/+}$ and *St3gal5*$^{-/-}$ mice, with (+) or without (-) rAAV9.CB.hST3GAL5 treatment. GD1a, GD1b, green; nuclei, counterstaining in blue. Quantification is in **Fig. S2**.

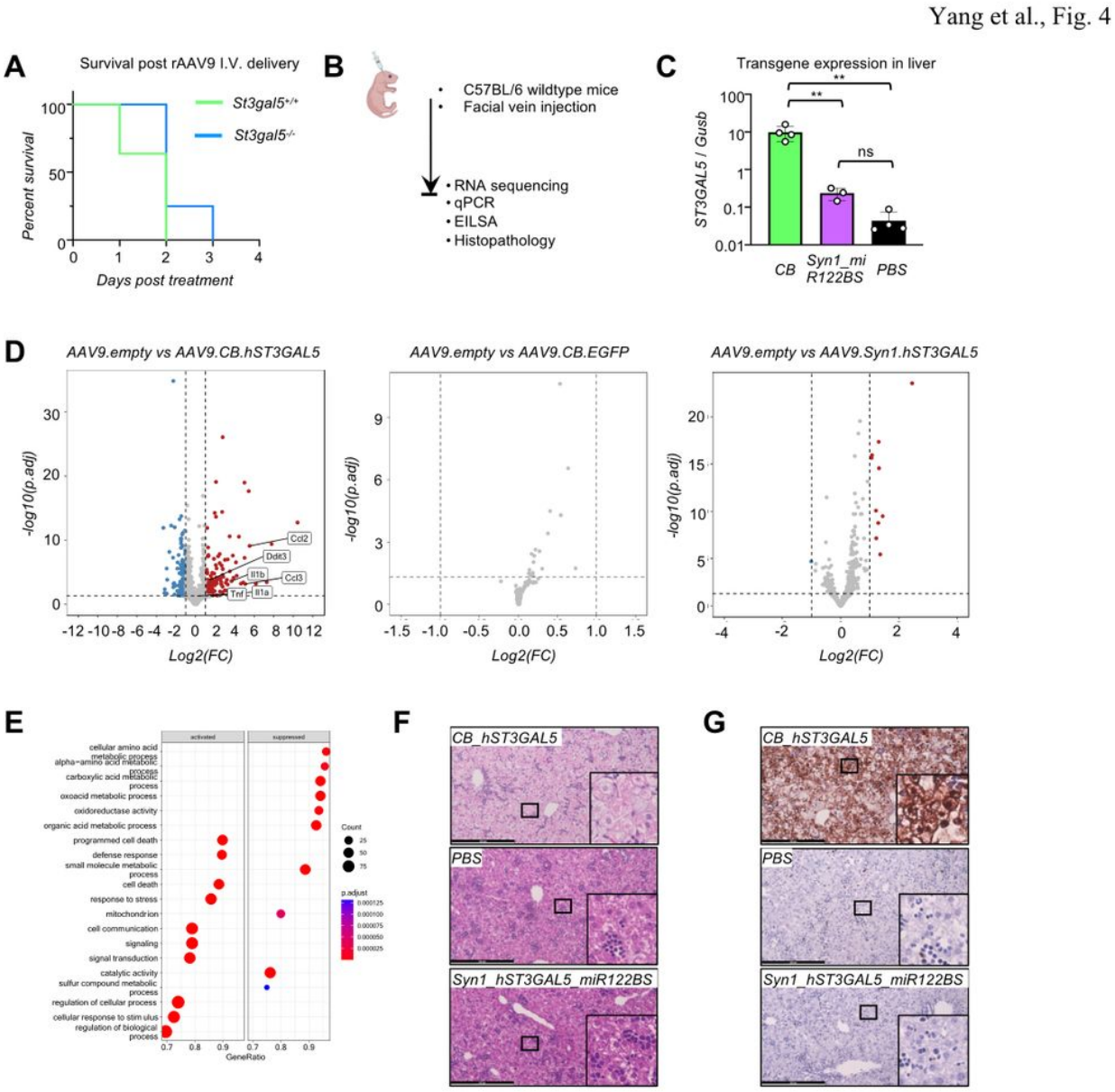

Figure 4

Liver de-targeting eliminates ST3GAL5 overexpression induced toxicity.

(**A**). Median survival of post AAV9.CB.hST3GAL5 intravenous (I.V.) delivery. Data are plotted as probability of survival from 4-11 animals. (**B**). Schematic of facial vein delivery of AAV9.CB.hST3GAL5, or AAV9. EGFP, or AAV9.empty, or AAV9.Syn1.hST3GAL5.miR122BS, or PBS in wildtype mice. (**C**). ddPCR quantification of human ST3GAL5 cDNA in the liver of wildtype mice with rAAV9.CB.hST3GAL5 or

rAAV9.hSyn1.hST3GAL5.miR122BS treatments and endogenous mouse St3gal5 from PBS treatment. Data are mean ± s.d. of 3-4 animals per group. Statistical analysis was performed by Student t-test. *p<0.05, **p<0.01. (**D**). Volcano plots showing differential expressed genes in mouse livers. Blue: down, Red: up, Grey: not significant. Adjusted P value <=0.05, foldchange >=2. (**E**). Graph depicting significantly enriched pathways for differential expressed genes between liver from wildtype mice injected with PBS and rAAV9.CB.hST3GAL5 using Gene Set enrichment analysis (GSEA). (**F**). Representative images of hematoxylin and eosin (H&E) staining of liver sections from wildtype mice injected with rAAV9.CB.hST3GAL5 or PBS or rAAV9.hSyn1.hST3GAL5.miR122BS. (**G**). Representative images of terminal deoxynucleotidyl transferase dUTP nick end labeling (TUNEL) staining of liver sections from wildtype mice injected with rAAV9.CB.hST3GAL5 or PBS or rAAV9.hSyn1.hST3GAL5.miR122BS.

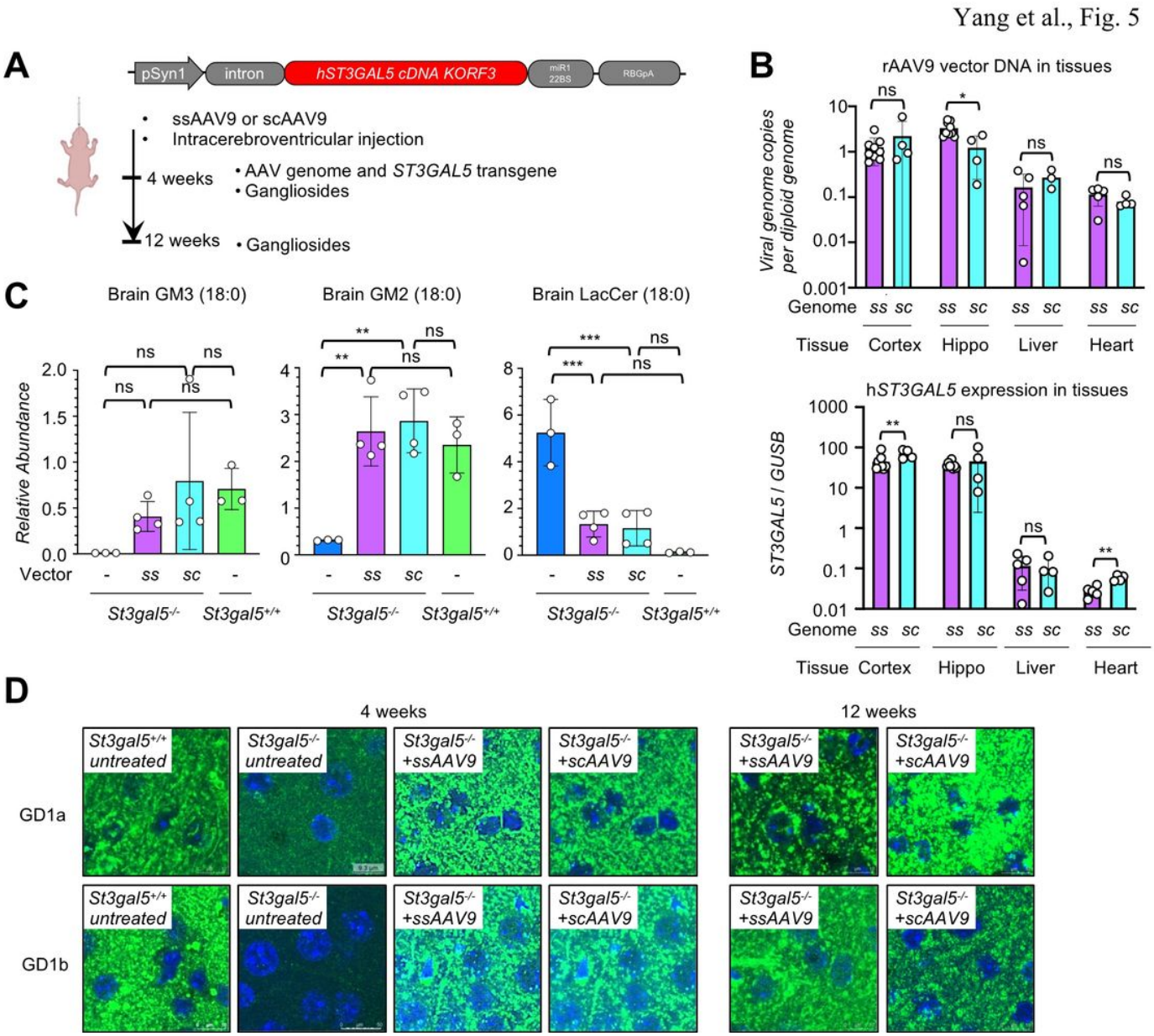

Figure 5

Second generation of *ST3GAL5* replacement vector restores gangliosides production in *St3gal5*$^{-/-}$ mouse model.

(**A**). Schematic of I.C.V. delivery of neuron-specific human *ST3GAL5* KORF3 (ST3GAL5.v2) in *St3gal5*$^{-/-}$ mouse model. (**B**). ddPCR quantification of rAAV9 genome and human *ST3GAL5* cDNA in the cortex, hippocampus (Hippo), liver and heart of ssAAV9.ST3GAL5.v2 or scAAV9.ST3GAL5.v2 treated *St3gal5*$^{-/-}$ mice. Data are mean ± s.d. of 4-9 animals per group. Statistical analysis was performed by student t-test. *p<0.05, **p<0.01, ns: not significant. (**C**). Mass Spectrometry (MS) quantification of GM3 (18:0), GM2 (18:0), and LacCer (18:0) from the brain of *St3gal5*$^{+/+}$ and *St3gal5*$^{-/-}$ mice, with ssAAV9.ST3GAL5.v2 or scAAV9.ST3GAL5.v2 or no treatment. Data are mean ± s.d. of 3-4 animals per group. Statistical analysis was performed by one-way ANOVA, followed by Sidak's multiple comparisons test. *p<0.05, **p<0.01, ***p<0.001, ns: not significant. (**D**). Representative images of major brain gangliosides in cortex of *St3gal5*$^{+/+}$ and *St3gal5*$^{-/-}$ mice, with ssAAV9.ST3GAL5.v2 or scAAV9.ST3GAL5.v2 or no treatment. GD1a, GD1b, green; nuclei, counterstaining in blue. Quantification is in **Fig. S2**.

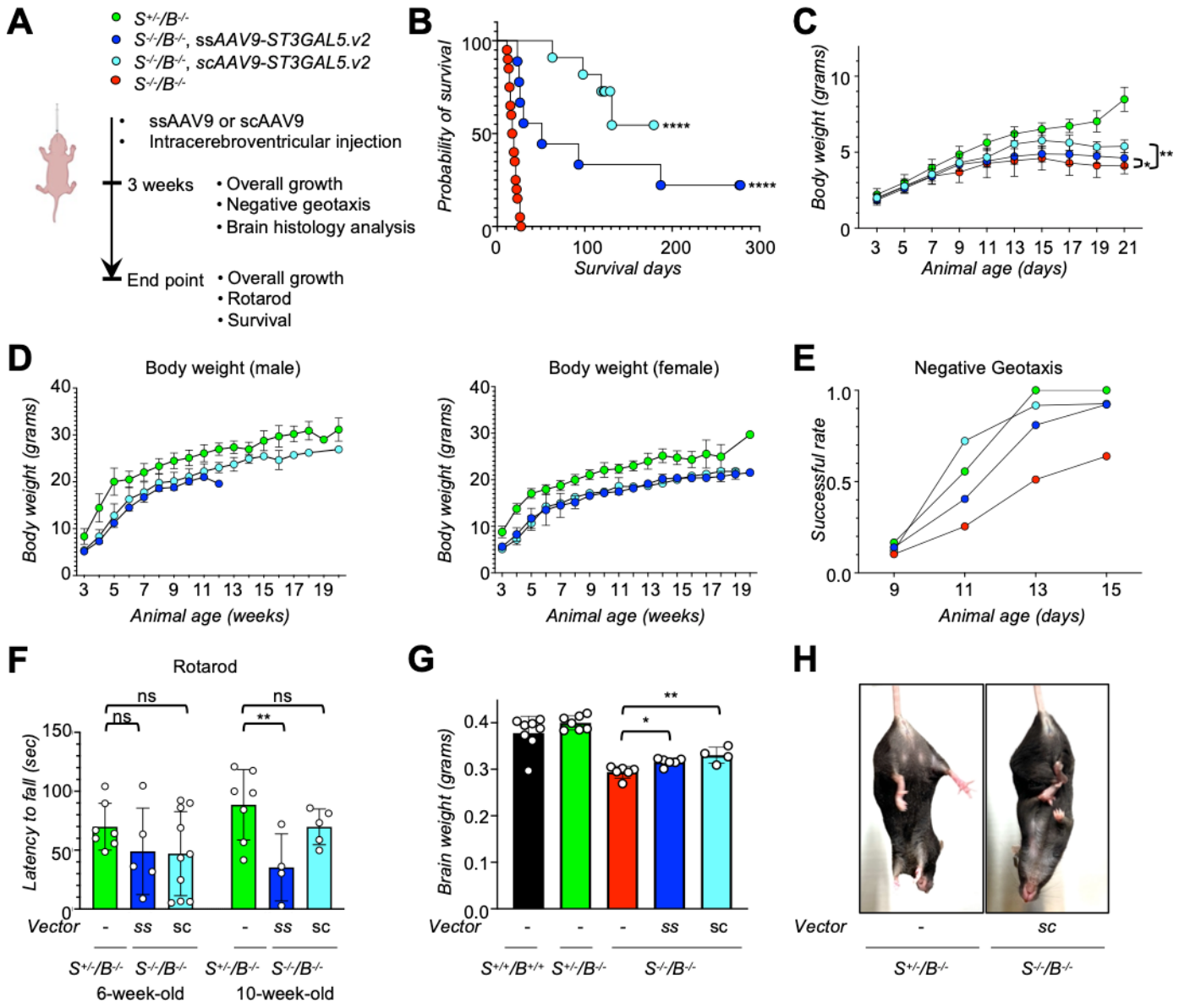

Figure 6

Second generation of *ST3GAL5* replacement vector rescues phenotypical changes in *St3gal5*$^{-/-}$*/B4galnt1*$^{-/-}$ mouse model.

(**A**). Schematic of I.C.V. delivery of rAAV-ST3GAL5.v2 in *St3gal5*$^{-/-}$*/B4galnt1*$^{-/-}$ mouse model. (**B**). Median survival of *St3gal5*$^{-/-}$*/B4galnt1*$^{-/-}$ mice, with ssAAV9.ST3GAL5.v2 or scAAV9.ST3GAL5.v2 or no treatments. Data are plotted as probability of survival from 7-20 animals. Statistical analysis was performed by Lon-rank (Mantel-Cox) test. ****p<0.0001. (**C**). A time course body weight from postnatal pups aging from 3 days old to 21 days old. Data are mean ± s.d. of 10 animals. Statistical analysis was performed by two-way ANOVA, followed by Sidak's multiple comparisons test. *p<0.05, **p<0.01. (**D**). Body weight at postweaning stage. Data are represented as mean ± s.d. of 5-8 animals. (**E**). Negative geotaxis successful rate from postnatal pups aging from 9 days old to 15 days old. Data are normalized

from 10 animals. (**F**). Quantification of rotarod assay for *St3gal5*$^{+/-}$*/B4galnt1*$^{-/-}$ mice and ssAAV9.ST3GAL5.v2 or scAAV9. T3GAL5.v2 treated *St3gal5*$^{-/-}$*/B4galnt1*$^{-/-}$ mice at 6 weeks old or 10 weeks old. Data are represented as mean ± s.d. of 4-7 animals. Statistical analysis was performed by one-way ANOVA, followed by Sidak's multiple comparisons test. ns: not significant, *p<0.05, **p<0.01. (**G**). Quantification of brain weight from wildtype mice or *St3gal5*$^{-/-}$*/B4galnt1*$^{-/-}$ mice, with ssAAV9.ST3GAL5.v2 or scAAV9.ST3GAL5.v2 or no treatments at 3 weeks old. Data are mean ± s.d. of 4-8 animals. Statistical analysis was performed by one-way ANOVA, followed by Sidak's multiple comparisons test. *p<0.05, **p<0.01. (**H**). Representative images of mouse hindlimb clasping from *St3gal5*$^{-/-}$*/B4galnt1*$^{-/-}$ mouse with scAAV9.ST3GAL5.v2 treatment or *St3gal5*$^{+/-}$*/B4galnt1*$^{-/-}$ mouse.

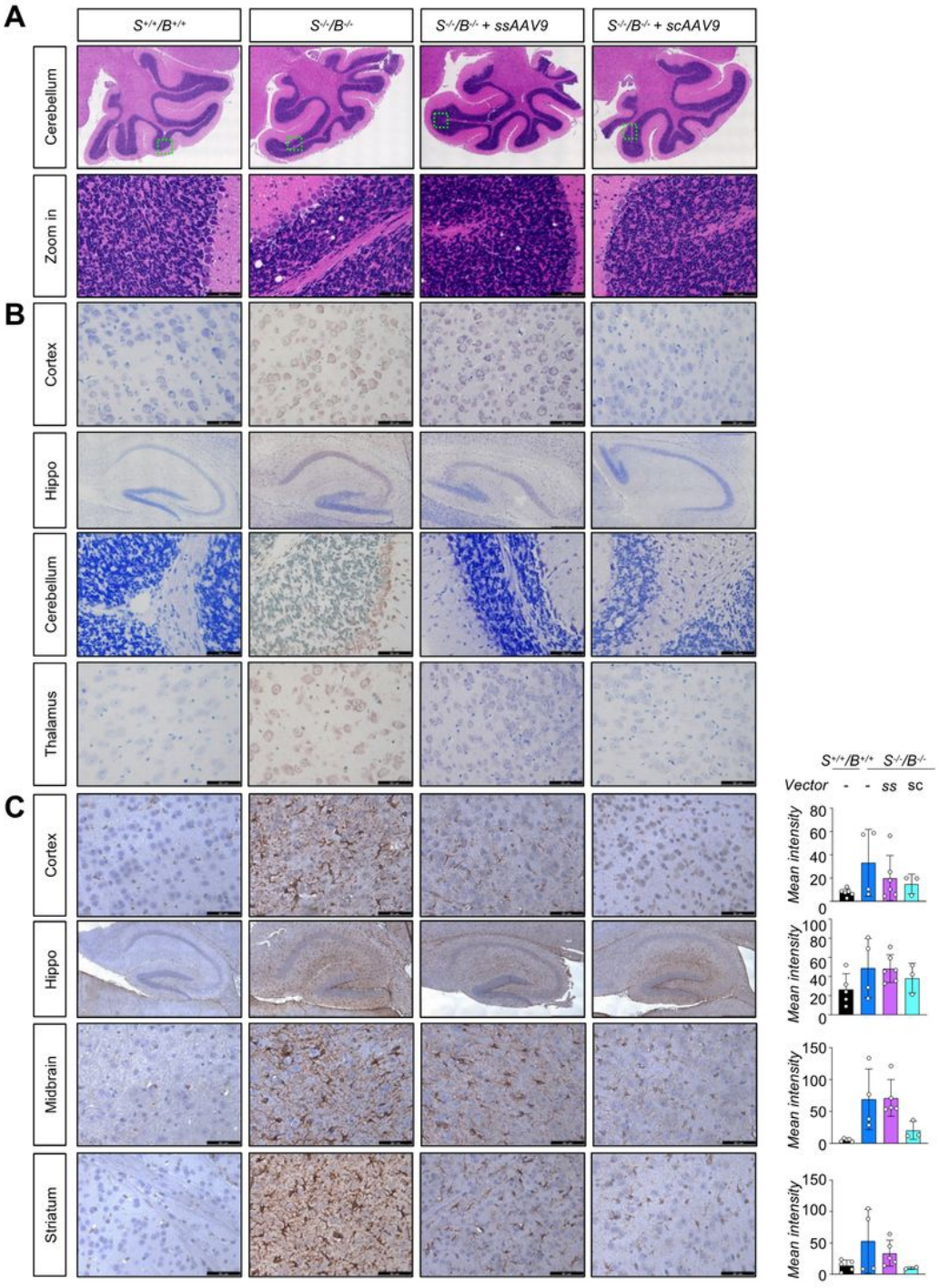

Figure 7

Second generation of *ST3GAL5* replacement vector rescues brain histology in *St3gal5*$^{-/-}$/*B4galnt1*$^{-/-}$ mouse model.

(**A**). Representative images of hematoxylin and eosin (H&E) staining of cerebellum sections from wildtype mice and *St3gal5*$^{-/-}$/*B4galnt1*$^{-/-}$ mice with ssAAV9.ST3GAL5.v2 or scAAV9.ST3GAL5.v2 or no treatments.

Black rectangle: zoom in area. (**B**). Representative images of terminal deoxynucleotidyl transferase dUTP nick end labeling (TUNEL) staining of brain sections (cortex, hippocampus, cerebellum) from wildtype mice and *St3gal5*$^{-/-}$/*B4galnt1*$^{-/-}$ mice with ssAAV9.ST3GAL5.v2 or scAAV9.ST3GAL5.v2 or no treatments. (**C**). Representative images and quantification of anti-GFAP immunostaining of brain sections (cortex, hippocampus, midbrain) from wildtype mice and *St3gal5*$^{-/-}$/*B4galnt1*$^{-/-}$ mice with ssAAV9.ST3GAL5.v2 or scAAV9.ST3GAL5.v2 or no treatments. Mean intensity was quantified by Fiji. Data are represented as mean ± s.d. of 3-5 animals. Statistical analysis was performed by one-way ANOVA, followed by Sidak's multiple comparisons test.

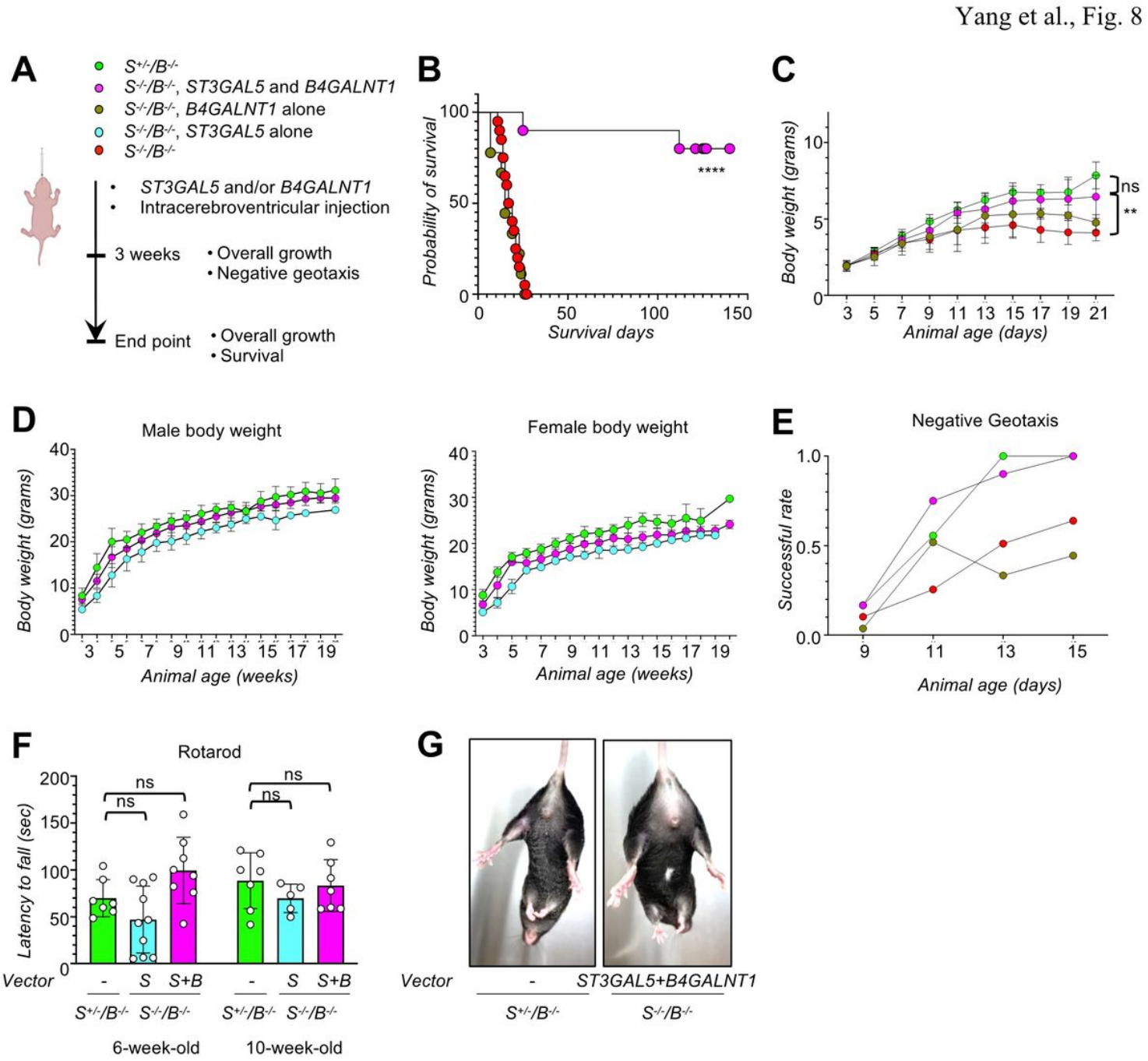

Figure 8

Co-delivery of *ST3GAL5* and *B4GALNT1* vectors normalize *St3gal5*$^{-/-}$/*B4galnt1*$^{-/-}$ mouse model.

(**A**). Schematic of I.C.V. co-delivery of AAV vectors expressing *ST3GAL5* and *B4GALNT1* cDNA respectively in *St3gal5*$^{-/-}$/*B4galnt1*$^{-/-}$ mouse model. (**B**). Median survival of *St3gal5*$^{-/-}$/*B4galnt1*$^{-/-}$ mice, with or without co-delivery of *ST3GAL5* and *B4GALNT1*. Data are plotted as probability of survival from 8-20 animals. Statistical analysis was performed by Lon-rank (Mantel-Cox) test. ****p<0.0001. (**C**). A time course body weight from postnatal pups aging from 3 days old to 21 days old. Data are mean ± s.d. of 10 animals. Statistical analysis was performed by two-way ANOVA, followed by Sidak's multiple comparisons test. *p<0.05, **p<0.01, ns: not significant. (**D**). Body weight of male and female at postweaning stage. Data are represented as mean ± s.d. of 3-5 animals. (**E**). Negative geotaxis successful rate from postnatal pups aging from 9 days old to 15 days old. Data are normalized from 7-9 animals. (**F**). Quantification of rotarod assay for *St3gal5*$^{+/-}$/*B4galnt1*$^{-/-}$ mice and ssAAV9.ST3GAL5.v2 or scAAV9.ST3GAL5.v2 or dual vectors treated *St3gal5*$^{-/-}$/*B4galnt1*$^{-/-}$ mice at 6 weeks old and 10 weeks old. Data are represented as mean ± s.d. of 5-8 animals. (**G**). Representative images of mouse hindlimb from *St3gal5*$^{-/-}$/*B4galnt1*$^{-/-}$ mouse with dual vectors treatment or *St3gal5*$^{+/-}$/*B4galnt1*$^{-/-}$ mouse.

Supplementary Files

This is a list of supplementary files associated with this preprint. Click to download.

- YangetalST3GL5supps.pdf